

797 **Chapter 3**
798 **Classical Cyclotron**

799 **Abstract** This tutorial is an introduction to the classical cyclotron, with hints at
800 spin dynamics, hands-on: by numerical simulation. It begins with a brief reminder
801 of the historical context, and then introduces the theoretical material needed for the
802 subsequent simulation exercises.

803
804 Basic charged particle optics and acceleration concepts are addressed in this chapter,
805 including

- 806 - closed orbit in a cyclic accelerator,
- 807 - weak focusing in a dipole magnet,
- 808 - periodic transverse motion,
- 809 - revolution period and isochronism,
- 810 - voltage gap and resonant acceleration,
- 811 - the cyclotron equation.

812
813 Simulations of a cyclotron dipole just requires the optical element DIPOLE, an
814 analytical modeling of the field. It may be chosen to use TOSCA however, if a
815 field map of the cyclotron magnet (computed or measured) is available. The only
816 other optical element which will be needed is CAVITE, to simulate an oscillating
817 voltage gap. Simulations also introduce to the default output listing zgoubi.res, to
818 optional output files such as zgoubi.plt produced by setting IL=2 in optical ele-
819 ments, zgoubi.CAVITE.out produced by CAVITE, zgoubi.MATRIX.out produced
820 by MATRIX, and other similar zgoubi.*.out output files aimed at data post-treatment,
821 including producing graphs. Additional keywords are introduced, including FIT[2],
822 a matching procedure; FAISCEAU which allows logging local particle coordinates
823 in zgoubi.res; FAISTORE which logs local particle coordinates in a user defined file,
824 usually for further external data treatment or plotting; MARKER; the 'system call'
825 command SYSTEM; REBELOTE, a 'do loop'; and some more. Spin motion will
826 be solved as well, this will require introducing SPNTRK, a request to do so while
827 raytracing, and SPNPRT which prints out spin vector components to zgoubi.res.

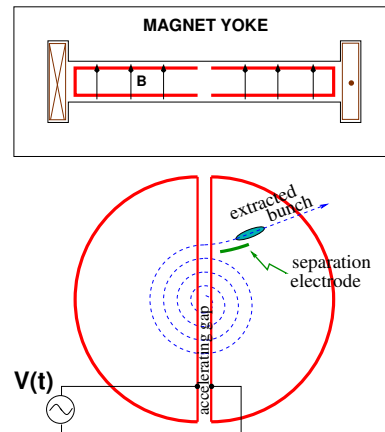
828 **Notations used in the Text**

$B; B_0$	field value; at reference radius R_0
$\mathbf{B}; B_R; B_y$	field vector; radial component; axial component
$B\rho = p/q$	particle rigidity
$C; C_0$	orbit length, $C = 2\pi R$; reference, $C_0 = 2\pi R_0$
E	particle energy
$f_{rf}; h$	RF frequency; RF harmonic number
$k = \frac{R}{B} \frac{dB}{dR}$	radial field index
$m; m_0; M$	mass; rest mass; in units of MeV/c^2
$\mathbf{p}; p; p_0$	particle momentum vector; its modulus; reference
q	particle charge
829 $R; R_0; R_E$	orbital radius; reference radius $R(p_0)$; at energy E
s	path variable
$\mathbf{v}; v$	particle velocity vector; its modulus
$V(t); \hat{V}$	oscillating voltage; its peak value
x, x', y, y'	radial and axial coordinates in the moving frame [$(*)' = d(*)/ds$]
$\beta = v/c; \beta_0; \beta_s$	normalized particle velocity; reference; synchronous
$\gamma = E/m_0$	Lorentz relativistic factor
$\Delta p, \delta p$	momentum offset
ϵ_u	Courant-Snyder invariant (u: x, r, y, l, Y, Z, s, etc.)
ϕ	RF phase at particle arrival at the voltage gap

830 **Introduction**

831 The cyclotron is the first cyclic accelerator. The concept: resonant acceleration of particles circling in a uniform magnetic field, goes back to the late 1920s [1]. The

Fig. 3.1 A sketch of the classical cyclotron. In the uniform magnetic field between two circular poles (top) an ion spirals out (bottom). A double-dee (or a single-dee facing a slotted electrode) forms a gap to which a fixed-frequency oscillating voltage $V(t)$ is applied. Its oscillation frequency is a harmonic of the revolution frequency. Particles experiencing proper voltage phase at the gap are accelerated. A septum electrode allows bunch extraction



832 first cyclotron was constructed at Berkeley, acceleration of H_2^+ hydrogen ions to
 833 80 keV [2] was achieved in 1931. The apparatus used a single dee vis-à-vis a slotted
 834 electrode forming a voltage gap, the ensemble housed in a 5 inch diameter vacuum
 835 chamber and placed in the 1.3 Tesla field of an electromagnet (Fig. 3.1). A \approx 12 MHz
 836 vacuum tube oscillator a 1 kVolt peak gap voltage.

837 The goal foreseen in developing this technology was the acceleration of protons
 838 to MeV kinetic energy range for the study of atom nucleus - and in background a
 839 wealth of potential applications. An 11 inch cyclotron delivering a $0.01 \mu A H_2^+$ beam
 840 at 1.22 MeV [3], and then a 27 inch cyclotron reaching 6 MeV (Fig. 3.2), followed [4].
 841 In the wake of Cockcroft and Walton first artificial disintegration experiment, targets
 842 were mounted at the periphery of the 11 inch cyclotron, disintegrations were observed
 843 in 1932. And in 1933: *'The neutron had been identified by Chadwick in 1932. By*
 844 *1933 we were producing and observing neutrons from every target bombarded by*
 845 *deuterons.* " [4, M.S. Livingston,p. 22].

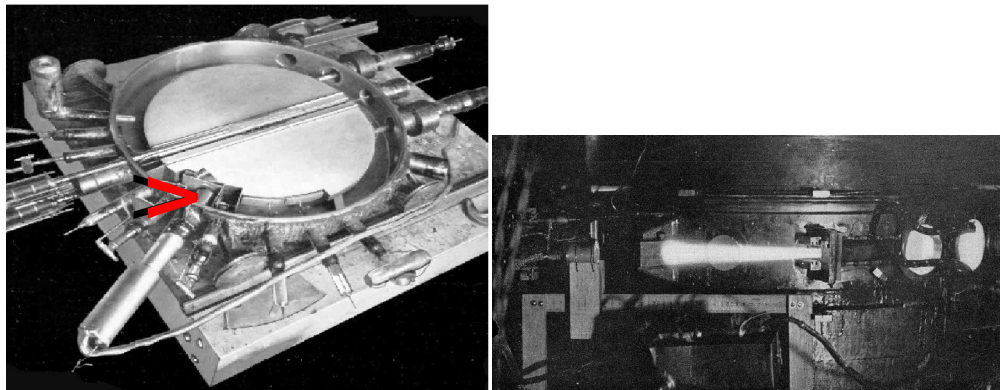


Fig. 3.2 Berkeley 27 inch cyclotron, first operated in 1934, accelerated deuterons up to 6 MeV. Left: a double-dee (seen in the vacuum chamber, cover off), 22 inch diameter, creates an accelerating gap: 13 kV, 12 MHz radio frequency voltage is applied for deuterons for instance (through two feed lines seen on the right). This apparatus was dipped in the 1.6 Tesla dipole field of a 27 in diameter (75 ton) electromagnet. A slight decrease of the dipole field with radius, from the center of the dees, assured vertical beam focusing. Particles spiral out from the center of the dees to the rim (where they strike a target, seen at the bottom on the left - arrow). Right: ionization of the air by the extracted beam (1936); the view also shows the vacuum chamber squeezed between the pole pieces of the electromagnet

846 The scope with accelerated beams from cyclotrons was broad: *"At this time*
 847 *biological experiments were started. I can recall the first time that a mouse was*
 848 *irradiated with neutrons. We put the mouse in a little cage and stuck him up on the*
 849 *side of the cyclotron tank and left him there for a while. Of course, nothing happened*
 850 *because [etc.]*" [4, McMillan,p.26]; and *"Also at about this same time the first*
 851 *radioactive tracer experiments on human beings were tried*" [op.cit.]; *"[...] simple*
 852 *beginnings of therapeutic use, coming a little bit later, in which neutron radiation was*
 853 *used, for instance, in the treatment of cancer. These things have gone on and built up*

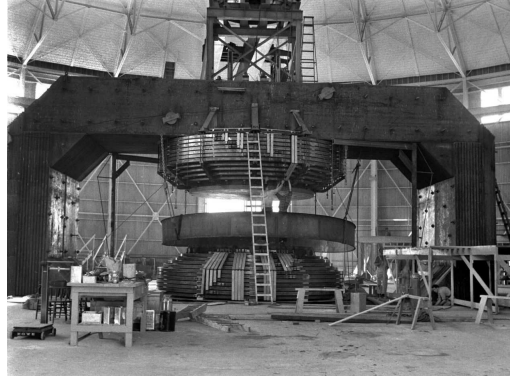


Fig. 3.3 Berkeley 184 in cyclotron. It was modified into a synchrocyclotron in 1946

854 *so that there's now a whole field*" [op.cit.]; and *"Another highlight from 1936 was the*
 855 *first time that anyone tried to make artificially a naturally occurring radionuclide."*
 856 (a bismuth isotope) [op.cit.]. The period also saw beam extraction developments
 857 (Fig. 3.2). Cyclotrons were constructed in many laboratories worldwide, from the
 858 early 1930s, following Berkeley demonstration.

859 *Limitation in energy*

860 An advanced theoretical understanding of the cyclotron more or less took until the
 861 mid-1930s, ending up with two news, a bad one and a good one, bad one first:

862 (i) the energy limitation, a consequence of the loss of isochronism resulting from
 863 the relativistic increase of the ion mass: "[...] *it seems useless to build cyclotrons of*
 864 *larger proportions than the existing ones [...] an accelerating chamber of 37 in radius*
 865 *will suffice to produce deuterons of 11 MeV energy which is the highest possible*
 866 *[...]*" [5] (related simulations will conclude this Chapter, "Classical Cyclotron"), or
 867 in a different form: *"If you went to graduate school in the 1940s, this inequality*
 868 *($-1 < k < 0$) was the end of the discussion of accelerator theory*" [6].

869 The good news next:

870 (ii) the overcoming of that relativistic limit, due to L.H. Thomas in 1938 [7] - it
 871 took a few years though, to see practical effects.

872 Classical cyclotron technology has been in use for some time up to the few tens
 873 of MeV/u that it allows (Fig. 3.4), for such applications as neutron production for
 874 material science, radio-isotope production for medicine, injector stages in cyclotron
 875 complex facilities [9]. However with the progress in magnet computation tools and
 876 magnet fabrication (including permanent magnet techniques [10]), and the progress
 877 in computational speed and beam dynamics simulations (which includes accurate
 878 raytracing, as concerned in the present opus), the azimuthally varying field (AVF,
 879 or Thomas' [7]) cyclotron, much more performing, comes out to be essentially as
 880 simple and has in a general manner prevailed (Fig. 3.4).

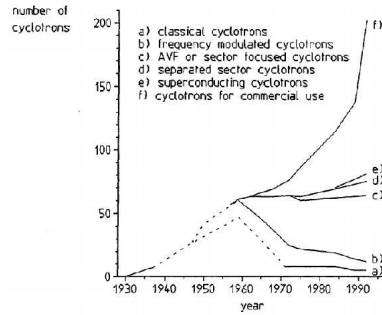
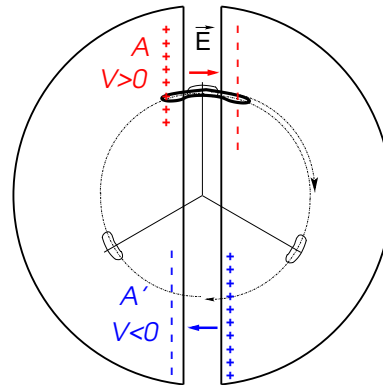


Fig. 3.4 Evolution of cyclotron species, over the years [8, Fig. 8]

881 **3.1 Theory, Basic Concepts**

882 The cyclotron was conceived as a means to overcome the inconvenient of using a
 883 long series of high voltage electrodes in a linear layout, by, instead, repeated re-
 884 circulation using a magnetic field, for incremental, resonant, energy gain through
 a single accelerating gap. This gap is formed by a pair of cylindrical electrodes,

Fig. 3.5 Resonant acceleration: a positive ion bunch meets an accelerating field **E** across gap A, at time *t*; it meets again, half a revolution later, at time $t + T_{rev}/2$, an accelerating field across gap A', and so on so forth. In this $h = 1$ configuration, one bunch (and only one) over a turn is in synchronism with the accelerating phase of the oscillating voltage, at both gaps. Higher *h* allows more bunches: the next possibility with two dees would be $h=3$, and three stable bunches at 120 degrees from one another (thin contours) over a turn



885 “dees” (Fig. 3.5) which are applied a fixed frequency oscillating voltage, generated
 886 using a radio transmitter. The dees are placed in a uniform magnetic field which
 887 causes the ion bunches to follow, as they are accelerated, a piecewise-circular motion
 888 with increasing radius, normal to the field, more or less in phase with the voltage
 889 oscillation. An oscillating voltage is necessary as a DC voltage gap (a conservative
 890 field) in a circular accelerator can not yield energy gain: with the advent of resonant
 891 acceleration in the cyclotron and the development of cyclic accelerators in the hori-
 892 zon, it is interesting to note in passing that it is not possible to accelerate a particle
 893

894 traveling on a closed path using an electrostatic field ($\mathbf{E} = -\mathbf{grad}V(\mathbf{R}, t)$ derives
 895 from a scalar potential), as the work by $\mathbf{F} = q\mathbf{E}$ only depends on the initial and final
 896 states, it does not dependent on the path followed (Fig. 3.6), which can be written

$$W = \int_P^Q \mathbf{F}.ds = -q \int_P^Q \mathbf{grad}V.ds = -q(V_Q - V_P) \quad (3.1)$$

897 On a closed path: $\oint \mathbf{F}.ds = 0$, the force is conservative, no work is performed,
 898 consequence: a DC voltage gap in a circular machine does not yield energy gain.

899 Instead, the work of a force of induction origin, where $\mathbf{E} = -\partial\mathbf{A}/\partial t$ arises from
 900 the variation of a magnetic flux ($\mathbf{B} = \mathbf{curl}\mathbf{A}$, \mathbf{A} a vector potential), may be non-zero
 901 on a closed path. This is achieved for instance using a radio-frequency system which
 902 feeds an oscillating voltage across a gap, $V(t) = \hat{V} \sin(\omega_{rf}t + \phi)$ (Fig. 3.7).

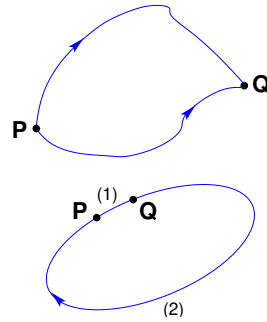


Fig. 3.6 Top: the work of the electrostatic force $\mathbf{F} = q\mathbf{E}$ is $W = \int_P^Q \mathbf{F}.ds = -q(V_Q - V_P)$. Bottom: over closed path, the particle loses along (2) the energy gained along (1)

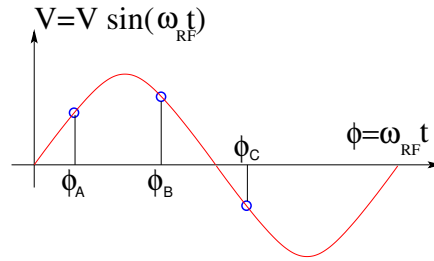


Fig. 3.7 A particle which reaches the double-dee gap at the RF phase $\omega_{rf}t = \phi_A$ or $\omega_{rf}t = \phi_B$ is accelerated. If it reaches the gap at $\omega_{rf}t = \phi_C$ it is decelerated

903 As an accelerated bunch spirals outward in a uniform magnetic field, the increase
 904 in the distance it travels over a turn is compensated by its velocity increase: in
 905 the non-relativistic approximation ($\beta \ll 1$), the revolution period T_{rev} increases
 906 only slowly with energy; with appropriate voltage frequency $f_{rf} \approx h/T_{rev}$ revolution
 907 motion and RF can be maintained in sufficiently close synchronism, $T_{rev} \approx hT_{rf}$, that
 908 the bunch will transit the accelerating gaps (Fig. 3.5) during the accelerating phase
 909 of the oscillating $V(t)$ (Fig. 3.7).

910 The orbital motion quantities: radius R , field B , particle rigidity BR , revolution
911 frequency $f_{\text{rev}} = \omega_{\text{rev}}/2\pi$, satisfy

$$BR = \frac{p}{q}, \quad 2\pi f_{\text{rev}} = \frac{v}{R} = \frac{qB}{m} = \frac{qB}{\gamma m_0} \quad (3.2)$$

These relationships hold at all γ , from $v \ll c$ ($\gamma \approx 1$, domain of the *classical* cyclotron) to $\gamma > 1$ (domain of the *isochronous* cyclotron). To give an idea of the revolution frequency, in the limit $\gamma = 1$ one has

$$\frac{f_{\text{rev}}}{B} = \frac{q}{2\pi m} = 15.25 \text{ MHz/T} \quad \text{for protons.}$$

912 The RF frequency $f_{\text{rf}} = \omega_{\text{rf}}/2\pi$ is constant in a cyclotron, whereas the revolution
913 period slowly increases with energy (Sec. 3.1.3). In the classical cyclotron f_{rf} is set,
914 by design, equal to hf_{rev} for an intermediate energy taken along the acceleration
915 cycle. The energy gain, or loss, by the particle when transiting the gap is

$$\Delta W = q\hat{V} \sin \phi(t) \quad \text{with } \phi(t) = \omega_{\text{rf}}t - \omega_{\text{rev}}t + \phi_0 \quad (3.3)$$

916 with ϕ its phase with respect to the RF signal at the gap (*e.g.*, ϕ_A , ϕ_B or ϕ_C in
917 Fig. 3.7) and ϕ_0 the value at $t = 0$, $\omega_{\text{rev}}t$ the orbital angle advance.

Fixed-frequency acceleration requires the RF and cyclotron frequencies to be matched to one another. However the relativistic increase of the mass upon velocity increase causes the revolution period to increase with momentum: in $T_{\text{rev}} = 2\pi m/qB$, B is almost constant and m increases, resulting in a turn-by-turn

$$\frac{\Delta T_{\text{rev}}}{T_{\text{rev}}} = \gamma - 1$$

918 The mis-match between the accelerating RF and cyclotron frequencies is a
919 turn-by-turn cumulative effect and sets a limit to the tolerable isochronism defect,
920 $\Delta T_{\text{rev}}/T_{\text{rev}} \approx 2 - 3\%$, or highest velocity $\beta = v/c \approx 0.22$. This results for instance in
921 a practical limitation of the “classical cyclotron” to an upper ≈ 25 MeV for protons,
922 and ≈ 50 MeV for D and α particles.

923 To conclude on these basis concepts regarding acceleration, multiple accelerating
924 gap structures is part of the evolutions of the classical cyclotron, where a “D” is
925 rather a “ Δ ” pattern, and towards high RF frequency harmonic. An example among
926 many others is, as an illustration, GANIL C0 injector with its 4 accelerating gaps
927 and h=4 and h=8 RF operation [9].

928 3.1.1 Fixed-Energy Orbits, Revolution Period

929 The differential equations of particle motion are established in the Serret-Frénet
930 frame, Sec. 3.1.2, however, some basic geometrical properties can be derived in the

931 laboratory frame, as follows. In the laboratory frame $(O;x,y,z)$, with $(O;x,z)$ the bend
 932 plane, assume $\mathbf{B}|_{y=0} = \mathbf{B}_y$. A particle is launched from the origin with a velocity
 933 $\mathbf{v} = (v \sin \alpha, 0, v \cos \alpha)$ at an angle α from the longitudinal axis z (Fig. 3.8).

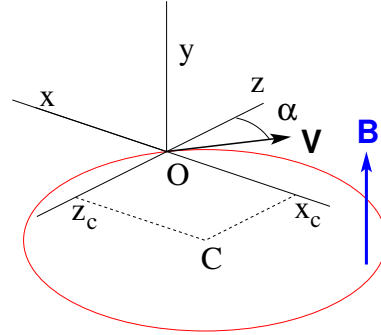


Fig. 3.8 Circular motion of a charged particle in the plane normal to a uniform magnetic field \mathbf{B} . The circle center is at $x_C = -v \cos \alpha / \omega_{rev}$, $z_C = v \sin \alpha / \omega_{rev}$.

934 Solving

$$m\dot{\mathbf{v}} = q\mathbf{v} \times \mathbf{B} \quad (3.4)$$

935 with $\mathbf{v} = (\dot{x}, \dot{y}, \dot{z})$, $\mathbf{B} = (0, B_y, 0)$ yields the parametric equations of motion

$$\begin{cases} x(t) = \frac{v}{\omega_{rev}} \cos(\omega_{rev}t - \alpha) - \frac{v \cos \alpha}{\omega_{rev}} \\ z(t) = \frac{v}{\omega_{rev}} \sin(\omega_{rev}t - \alpha) + \frac{v \sin \alpha}{\omega_{rev}} \\ y(t) = \text{constant} \end{cases} \quad (3.5)$$

936 which results in

$$\left(x + \frac{v \cos \alpha}{\omega_{rev}}\right)^2 + \left(z - \frac{v \sin \alpha}{\omega_{rev}}\right)^2 = \left(\frac{v}{\omega_{rev}}\right)^2 \quad (3.6)$$

a circular trajectory of radius $R = p/qB$ centered at $x = -v \cos \alpha / \omega_{rev}$, $z = v \sin \alpha / \omega_{rev}$, revolution period

$$T_{rev} = \frac{2\pi}{\omega_{rev}} = \frac{2\pi m}{qB}$$

937 *Cyclic motion* - Horizontal motion in uniform field has no privileged reference orbit:
 938 for a given momentum, the initial radius and velocity vector define a particular closed,
 939 circular orbit. A particle launched with an axial velocity component v_y , on the other
 940 hand, drifts vertically linearly with time, as there is no axial restoring force. The next

941 Section will investigate the necessary field property, absent in our simplified field
 942 model so far, proper to ensure confinement of the multiturn 6-dimensional periodic
 943 motion in the vicinity of the median plane of the cyclotron dipole magnet.

944 3.1.2 Weak Focusing, Transverse Motion

945 In the lower energy (smaller radius) accelerated turns in a classical cyclotron, the
 946 electric field in the accelerating gap contributes proper transverse focusing so that
 947 the magnet gap can be designed parallel (an example can be found in Ref. [9]). In
 948 very low energy applications even, extraction energy in the tens of keV/u range where
 949 electric fields are still effective, flat magnetic field with uniformity $dB/B < 10^{-4}$
 950 can be achieved over the (reduced) extent of the cyclotron orbit and maintains proper
 951 isochronism. Beyond this low energy region however, at greater radius, a magnetic
 952 field gradient must be introduced, field decreasing with R, by shaping the magnet
 953 poles, to ensure proper vertical focusing. Note that because of the field decreases
 954 with R in a parallel gap, as discovered *a posteriori*, the very first cyclotrons were
 955 working [11]. This section introduces to these magnetic focusing principles.

956 In the following, $B_R(R)$, $B_y(R)$ denote the radial and axial components of the
 957 magnetic field at radius R. Median-plane symmetry of the field is assumed, thus
 958 $B_R|_{y=0} = 0$ at all R (Fig. 3.9). Particle coordinates are defined in the Serret-Frénet
 959 frame (O;s,x,y), moving along the R_0 radius reference orbit (the origin O is at the
 960 location of the reference particle, s axis tangent to the reference orbit, x axis radial,
 961 y axis normal to the bend plane, Fig. 3.10). The radial excursion of a particle with
 962 respect to the reference orbit writes

$$x(t) = R(t) - R_0 \ll R_0 \quad (3.7)$$

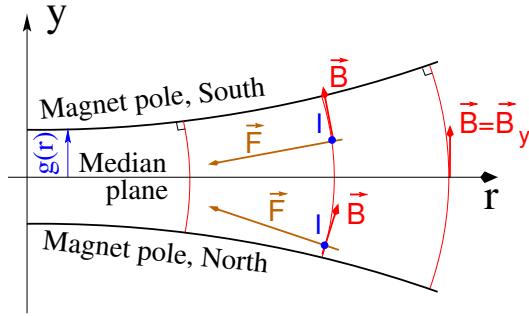
963 Considering small radial and axial excursions from ($R = R_0, y = 0$), a Taylor
 964 expansion of the magnetic field can be introduced,

$$\begin{aligned} B_y(R_0 + x) &= B_y(R_0) + x \left. \frac{\partial B_y}{\partial R} \right|_{R_0} + \frac{x^2}{2!} \left. \frac{\partial^2 B_y}{\partial R^2} \right|_{R_0} + \dots \approx B_y(R_0) + x \left. \frac{\partial B_y}{\partial R} \right|_{R_0} \\ B_R(0 + y) &= y \underbrace{\left. \frac{\partial B_R}{\partial y} \right|_0}_{= \left. \frac{\partial B_y}{\partial R} \right|_{R_0}} + \frac{y^3}{3!} \left. \frac{\partial^3 B_R}{\partial y^3} \right|_0 + \dots \approx y \left. \frac{\partial B_y}{\partial R} \right|_{R_0} \end{aligned} \quad (3.8)$$

965 Using this approximation, the differential equations of motion in the moving frame
 966 can be written under the form, linear in x and y ,

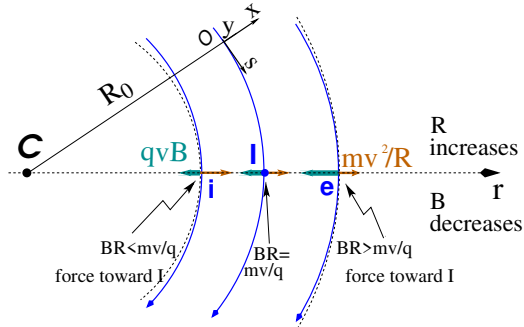
$$\begin{aligned}
 F_x = m\ddot{x} &= -qvB_y(R) + \frac{mv^2}{R_0 + x} \approx -qv \left(B_y(R_0) + \left. \frac{\partial B_y}{\partial R} \right|_{R_0} x \right) + \frac{mv^2}{R_0} \left(1 - \frac{x}{R_0} \right) \\
 \rightarrow m\ddot{x} &= -\frac{mv^2}{R_0^2} \left(\frac{R_0}{B_0} \left. \frac{\partial B_y}{\partial R} \right|_{R_0} + 1 \right) x \tag{3.9} \\
 F_y = m\ddot{y} &= qvB_R(y) = qv \left. \frac{\partial B_R}{\partial y} \right|_{y=0} y + \text{higher order} \rightarrow m\ddot{y} = qv \frac{\partial B_y}{\partial R} y
 \end{aligned}$$

Fig. 3.9 Axial motion stability requires proper shaping of field lines: B has to decrease with radius. The Laplace force pulls a charge at I (velocity pointing out of the page) toward the median plane. Increasing the field gradient (k closer to -1, gap opening up faster) increases the focusing



967

Fig. 3.10 Radial motion stability in an axially symmetric structure. Arrowed arcs are trajectories of particles with momentum $p=mv$. Dashed arcs are centered at C, center of the cyclotron. The resultant $F_t = -qvB + mv^2/r$, is zero at I: $B_0R_0 = mv/q$. The resultant at i is toward I if $qvB_i < mv^2/R_i$, i.e. $B_iR_i < mv/q$; the resultant at e is toward I if $qvB_e > mv^2/R_e$, i.e. $B_eR_e > mv/q$



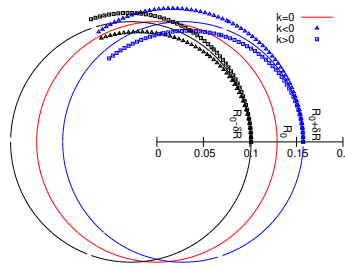
968 Note $B_y(R_0) = B_0$ and introduce

$$\omega_R^2 = \omega_{\text{rev}}^2 \left(1 + \frac{R_0}{B_0} \frac{\partial B_y}{\partial R} \right), \quad \omega_y^2 = -\omega_{\text{rev}}^2 \frac{R_0}{B_0} \frac{\partial B_y}{\partial R} \tag{3.10}$$

969 equations 3.9 can thus be written under the form

$$\ddot{x} + \omega_R^2 x = 0 \quad \text{and} \quad \ddot{y} + \omega_y^2 y = 0 \tag{3.11}$$

Fig. 3.11 Geometrical focusing: in a flat field, $k=0$, the two circular trajectories at $r = R_0 \pm \delta R$ (solid lines) undergo exactly one oscillation around the reference orbit $r = R_0$. A positive k increases the convergence (square markers - but then the vertical motion diverges from the median plane), a negative k decreases the convergence (triangles)



970 A restoring force (linear terms in x and y , Eq. 3.11) arises from the radially varying
 971 field, characterized by a field index

$$k = \frac{R_0}{B_0} \left. \frac{\partial B_y}{\partial R} \right|_{R=R_0, y=0} \quad (3.12)$$

972 and adds in the radial motion to the focusing due to the curvature (the term “1” in
 973 ω_R^2 , Eq. 3.10).

974 *Axial stability* in a cyclotron requires a restoring force directed toward the median
 975 plane. Referring to Fig. 3.9, this means $F_y = -ay$ (with the a factor some positive
 976 quantity) and thus $B_R < 0$, at all $(r, y \neq 0)$. This is achieved by designing a guiding
 977 field which decreases with radius, $\frac{\partial B_R}{\partial y} < 0$. Referring to Eq. 3.12 this translates into
 978 $k < 0$.

979 *Radial stability* in a constant field is a geometrical property, resulting from the
 980 curvature of the trajectory (Fig. 3.11). In a weakly decreasing field $B(R)$ on the
 981 other hand, a particle with momentum $p = mv$ sinusoiding around the R_0 -radius
 982 reference circle experiences in the Serret-Frénet frame a total force $F_t = -qvB + m \frac{v^2}{r}$
 983 (Fig. 3.10) of which the (outward) component $f_c = m \frac{v^2}{r}$ decreases with r at a higher
 984 rate than the decrease of the Laplace (inward) component $f_B = -qvB(r)$. In other
 985 words, radial stability requires BR to increase with R , $\frac{\partial BR}{\partial R} = B + R \frac{\partial B}{\partial R} \geq 0$, this
 986 holds in particular at R_0 , thus $1 + k \geq 0$.

987 The condition for transverse motion stability around the circular equilibrium orbit
 988 results from these axial and radial stability conditions, namely,

$$-1 \leq k < 0 \quad (3.13)$$

Note regarding the geometrical focusing: the focal distance associated with the curvature of a magnet of arc length \mathcal{L} is obtained by integrating $\frac{d^2x}{ds^2} + \frac{1}{R_0^2}x = 0$ and identifying with the focusing property $\Delta x' = -x/f$, namely,

$$\Delta x' = \int \frac{d^2x}{ds^2} ds \approx \frac{-x}{R^2} \int ds = \frac{-x\mathcal{L}}{R^2}, \text{ thus } f = \frac{R^2}{\mathcal{L}}$$

989 Isochronism

990 The relativistic increase of the mass precludes strict isochronism: the revolution
 991 frequency slowly decreases with the energy of the particle on its spiraling out
 992 trajectory (Eq. 3.2). The focusing condition $-1 < k < 0$ (B decreasing with R) further
 993 contributes breaking the isochronism by virtue of $\omega_{\text{rev}} \propto B$. As a consequence, the
 994 phase of the oscillating voltage at arrival of a particle at the accelerating gap (the
 995 so-called RF phase) changes turn after turn. This is addressed further in Sec. 3.1.3.

996 Paraxial Transverse Coordinates

997 Introducing the path variable, s , as the independent variable in Eq. 3.11 and using
 998 the approximation $ds \approx v dt$ (*i.e.*, neglecting the transverse velocity components), the
 999 equations of motion in the moving frame (Eq. 3.11) take the form

$$\frac{d^2x}{ds^2} + \frac{1+k}{R_0^2}x = 0 \quad \text{and} \quad \frac{d^2y}{ds^2} - \frac{k}{R_0^2}y = 0 \quad (3.14)$$

1000 Given $-1 < k < 0$ the motion is that of a harmonic oscillator, in both planes, with
 1001 respective restoring constants $(1+k)/R_0^2$ and $-k/R_0^2$, both positive quantities. The
 1002 solution is a sinusoidal motion,

$$\begin{cases} R(s) - R_0 = x(s) = x_0 \cos \frac{\sqrt{1+k}}{R_0}(s - s_0) + x'_0 \frac{R_0}{\sqrt{1+k}} \sin \frac{\sqrt{1+k}}{R_0}(s - s_0) \\ R'(s) = x'(s) = -x_0 \frac{\sqrt{1+k}}{R_0} \sin \frac{\sqrt{1+k}}{R_0}(s - s_0) + x'_0 \cos \frac{\sqrt{1+k}}{R_0}(s - s_0) \end{cases} \quad (3.15)$$

1003

$$\begin{cases} y(s) = y_0 \cos \frac{\sqrt{-k}}{R_0}(s - s_0) + y'_0 \frac{R_0}{\sqrt{-k}} \sin \frac{\sqrt{-k}}{R_0}(s - s_0) \\ y'(s) = -y_0 \frac{\sqrt{-k}}{R_0} \sin \frac{\sqrt{-k}}{R_0}(s - s_0) + y'_0 \cos \frac{\sqrt{-k}}{R_0}(s - s_0) \end{cases} \quad (3.16)$$

1004 The dissymmetry between the two frequencies, a “1” in “ $\sqrt{1+k}$ ” compared to $\sqrt{-k}$,
 1005 stems from the geometrical focusing resulting from the curvature.

1006 Two wave numbers may be introduced,

$$\nu_R = \frac{\omega_R}{\omega_{\text{rev}}} = \sqrt{1+k} \quad \text{and} \quad \nu_y = \frac{\omega_y}{\omega_{\text{rev}}} = \sqrt{-k} \quad (3.17)$$

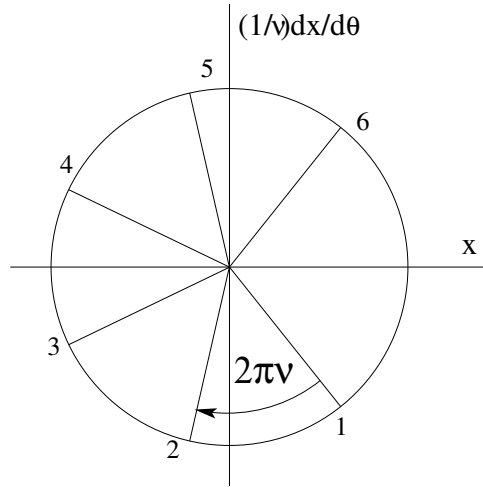
1007 *i.e.*, the number of sinusoidal oscillations of the paraxial motion about the reference
 1008 circular orbit over a turn, respectively radial and axial. Both are less than 1: there
 1009 is less than one sinusoidal oscillation in a revolution. In addition, as a result of the
 1010 revolution symmetry,

$$v_R^2 + v_y^2 = 1 \tag{3.18}$$

1011 **Phase Space**

1012 Phase space at an azimuth s around the ring is a Cartesian space with, regarding
 1013 transverse particle motion, position as the horizontal axis and angle as the vertical
 1014 axis, *i.e.*, $(x(s), x'(s) = dx/ds)$ and $(y(s), y'(s) = dy/ds)$ (Eqs. 3.15 3.16), or akin
 1015 quantities, this is illustrated in Fig. 3.12.

Fig. 3.12 Particle motion observed in transverse horizontal phase space at some fixed azimuth $s = R\theta_{\text{obs}}$ along the cyclotron circumference, at successive times (or turns: 1, 2, 3, ...). The horizontal axis here is $x(\theta_{\text{obs}})$, the vertical axis is $\left. \frac{1}{v_R} \frac{dx}{d\theta} \right|_{\theta=\theta_{\text{obs}}}$, using these coordinates the motion is on a circle of radius \hat{x} . Note that $\{x(\theta_{\text{obs}}) = \hat{x} \cos(\nu_R \theta_{\text{obs}} + \phi)$ and $\left. \frac{1}{v_R} \frac{dx}{d\theta} \right|_{\theta=\theta_{\text{obs}}} = -\hat{x} \sin(\nu_R \theta_{\text{obs}} + \phi)\}$ establishes that phase space motion is clockwise



1016 Longitudinal phase space coordinates are the RF phase ϕ (Fig. 3.7, Eq. 3.3) and
 1017 energy offset, or akin quantities.

1018 A point in phase space represents the position of a particle at azimuth s at time t .

1019 Particle motion over time depends on the field experienced and on two initial
 1020 conditions (initial position and angle, or RF phase and energy offset, ...). It is
 1021 impossible for two trajectories with different origins to coincide in phase space, at
 1022 any azimuth.

1023 **Off-Momentum Motion**

1024 Momenta of particles that make up a bunch accelerated in a cyclotron span some
 1025 extent $\pm \Delta p/p$.

In an axially symmetric structure, the equilibrium trajectory at momentum
 $\begin{cases} p_A \\ p_B = p_A + \Delta p \end{cases}$ is at radius $\begin{cases} R_A \text{ such that } B_A R_A = p_A/q \\ R_B \text{ such that } B_B R_B = p_B/q \end{cases}$, with $\begin{cases} B_B = B_A + \left(\frac{\partial B}{\partial x}\right)_0 + \dots \\ R_B = R_A + \Delta x \end{cases}$

On the other hand

$$B_B R_B = \frac{p_B}{q} \Rightarrow \left[B_A + \left(\frac{\partial B}{\partial x} \right)_0 \Delta x + \dots \right] (R_A + \Delta x) = \frac{p_A + \Delta p}{q} = \frac{p_A}{q} + \frac{\Delta p}{q}$$

thus, neglecting terms in $(\Delta x)^2$,

$$B_A R_A + \left(\frac{\partial B}{\partial x} \right)_0 R_A \Delta x + B_A \Delta x = \frac{p_A}{q} + \frac{\Delta p}{q},$$

1026 which, given $B_A R_A = \frac{p_A}{q}$, leaves $\Delta x \left[\left(\frac{\partial B}{\partial x} \right)_A R_A + B_A \right] = \frac{\Delta p}{q}$, which given $k =$
 1027 $\frac{R_A}{B_A} \left(\frac{\partial B}{\partial x} \right)_0$ yields

$$\Delta x = \frac{R_A}{1 + k} \frac{\Delta p}{p_A} \quad (3.19)$$

Drop the indices, take p as a reference momentum and R as the corresponding

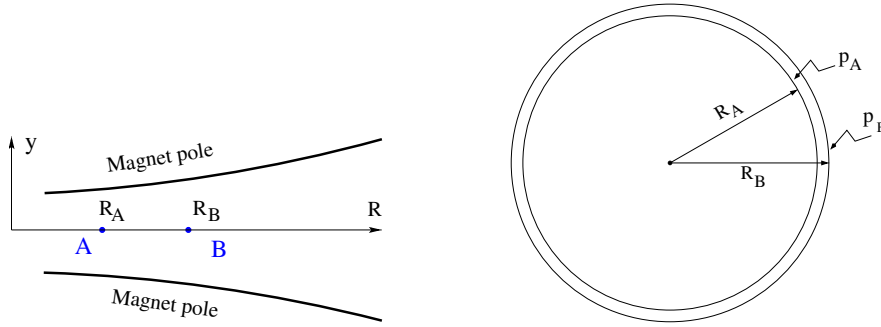


Fig. 3.13 The equilibrium radius at location A is $R = R_A$, the equilibrium momentum is p_A , rigidity $BR = B_A R_A$. The equilibrium radius at B is $R = R_B$, equilibrium momentum p_B , rigidity $BR = B_B R_B$

1028 reference orbit radius, this leaves
 1029

$$\Delta x = D \frac{\Delta p}{p} \quad \text{with} \quad D = \frac{R}{1 + k}, \quad \text{dispersion function} \quad (3.20)$$

1030 The dispersion D is an s -independent quantity in the classical cyclotron as a result of
 1031 the cylindrical symmetry of the field (k and $R=p/qB$ are s -independent), and varies
 1032 with R and $k(R)$.

1033 To the first order in the coordinates, the vertical coordinates $y(s)$, $y'(s)$ (Eq. 3.16)
 1034 are unchanged under the effect of a momentum offset, the horizontal trajectory angle
 1035 $x'(s)$ is unchanged as well (the circular orbits are concentric, Fig. 3.13) whereas

$$x(s, p + \Delta p) = x(s, p) + \Delta p \left. \frac{dx}{dp} \right|_{s,p} = x(s) + D \frac{\Delta p}{p} \quad (3.21)$$

1036 with $x(s)$ as in Eq. 3.15.

1037 *Orbit and revolution period lengthening*

1038 Momentum offset results in closed orbit lengthening $\delta C/C = \delta R/R \equiv \delta x/R$, which,
1039 given Eq. 3.20, can be written under the form

$$\frac{\delta C}{C} = \alpha \frac{\delta p}{p} \quad \text{with} \quad \alpha = \frac{1}{1+k} = \frac{1}{\gamma^2} \quad (3.22)$$

1040 with α the ‘‘momentum compaction’’ and $\alpha > 0$, the closed orbit length increases
1041 with momentum.

1042 The change in revolution period $T_{\text{rev}} = C/\beta c$ with momentum writes

$$\frac{\delta T_{\text{rev}}}{T_{\text{rev}}} = \frac{\delta C}{C} - \frac{\delta \beta}{\beta} = \left(\alpha - \frac{1}{\gamma^2}\right) \frac{\delta p}{p} \quad (3.23)$$

1043 Given that $-1 < k < 0$ and $\gamma \gtrsim 1$, it results that $\alpha - 1/\gamma^2 > 0$ thus $\delta T_{\text{rev}}/T_{\text{rev}} > 0$ as
1044 expected: the revolution period increases with energy, the increase in radius is faster
1045 than the velocity increase.

1046 3.1.3 Quasi-Isochronous Resonant Acceleration

1047 An oscillating radio-frequency (RF) electric field, with fixed-frequency f_{rf} is applied
1048 across the gap between the two dees (Fig. 3.1). An ion of charge q reaching the gap
1049 at time t undergoes a change in energy

$$\Delta W(t) = q\hat{V} \sin \phi, \quad \text{with} \quad \phi = \omega_{\text{rf}}t - (\omega_{\text{rev}}t + \phi_0) \quad (3.24)$$

1050 with ϕ the RF phase experienced by the particle at the time it crosses the gap and ϕ_0
1051 the origin in phase for the particle motion. This ignores the ‘‘transit time’’, the effect
1052 of the time that the particle spends across the gap on the overall energy gain.

1053 The frequency dependence of the kinetic energy W of the ion relates to its orbital
1054 radius R in the following way:

$$W = \frac{1}{2}mv^2 = \frac{1}{2}m(2\pi R f_{\text{rev}})^2 = \frac{1}{2}m(2\pi R \frac{f_{\text{rf}}}{h})^2 \quad (3.25)$$

1055 thus, given cyclotron size (R), f_{rf} and h set the limit for the acceleration range.

1056 The revolution frequency decreases with energy and the condition of synchronism
1057 with the oscillating voltage, $f_{\text{rf}} = hf_{\text{rev}}$, is only fulfilled at one particular radius in the
1058 course of acceleration, where $\omega_{\text{rf}} = qB/m$ (Fig. 3.14). Upstream and downstream
1059 of that radius, out-phasing $\Delta\phi$ builds-up turn after turn, decreasing in a first stage

1060 (towards lower voltages in Fig. 3.14-right) and then increasing back to $\phi = \pi/2$ and beyond towards π . Beyond $\phi = \pi$ the RF voltage is decelerating.

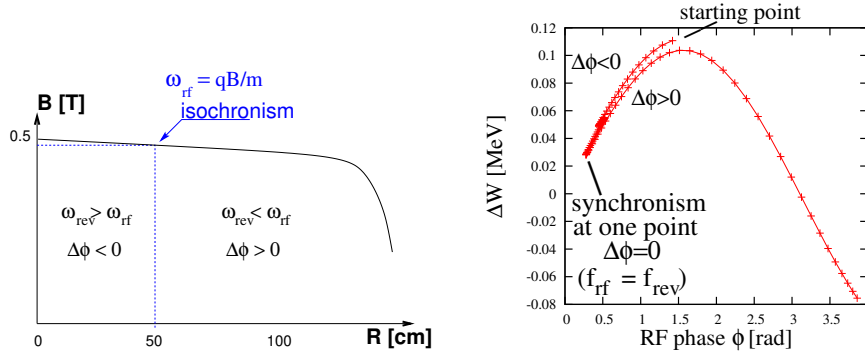


Fig. 3.14 A sketch of the synchronism condition at one point (left, $h=1$ assumed), and the span in phase of the energy gain $\Delta W = q\hat{V} \sin \phi$ over the acceleration cycle (right). ϕ is the phase of the RF sine wave at arrival of the particle at the accelerating gap (the vertical separation of the two $\Delta W(\phi)$ branches on the right ($\Delta\phi < 0$ and $\Delta\phi > 0$) is artificial, this is for clarity, they are actually superimposed)

1061

1062

1063

1064

Differentiating the particle phase at the RF gap (Eq. 3.24), over a half-turn, with ω_{rev} constant between two gap passages, one gets $\dot{\phi} = \omega_{rf} - \omega_{rev}$. Between two gap passages on the other hand, $\Delta\phi = \dot{\phi}\Delta T = \dot{\phi}T_{rev}/2 = \dot{\phi}\frac{\pi R}{v}$, yielding a phase-shift of

$$\text{half-turn } \Delta\phi = \pi \left(\frac{\omega_{rf}}{\omega_{rev}(R)} - 1 \right) = \pi \left(\frac{m\omega_{rf}}{qB(R)} - 1 \right) \quad (3.26)$$

1065

1066

1067

1068

1069

1070

1071

1072

The out-phasing is thus a gap-after-gap, cumulative effect. Due to this the classical cyclotron requires quick acceleration (limited number of turns), which means high voltage (tens to hundreds of kVolts). As expected, with ω_{rf} and B constant, ϕ presents a minimum ($\dot{\phi} = 0$) at $\omega_{rf} = \omega_{rev} = \frac{qB}{m}$ where exact isochronism is reached (Fig. 3.14). The upper limit to ϕ is set by the condition $\Delta W > 0$: acceleration.

The cyclotron equation determines the achievable energy range, depending on the injection energy E_0 , the RF phase at injection ϕ_0 , the RF frequency ω_{rf} and gap voltage \hat{V} , following [12]

$$\cos \phi = \cos \phi_0 + \pi \left[1 - \frac{\omega_{rf}}{\omega_{rev}} \frac{E + E_0}{2M} \right] \frac{E - E_0}{q\hat{V}} \quad (3.27)$$

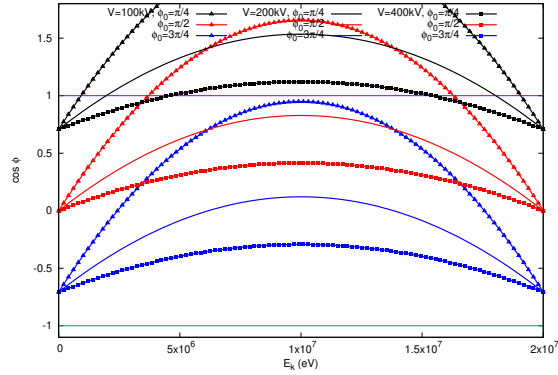
1073

1074

1075

($E=E_k + M$ is the total energy, M is the rest mass, the index 0 denotes injection parameters) and is represented in Fig. 3.15 for various values of the RF voltage and phase at injection ϕ_0 .

Fig. 3.15 A graph of the cyclotron equation (Eq. 3.27), for a few different RF settings. The sole settings resulting in a $\cos \phi$ curve comprised in $[-1, 1]$ allow complete acceleration from injection to top energy. For instance, for injection $\phi_0 = \pi/4$, acceleration to 20 MeV is not possible (upper three curves). Acceleration to 20 MeV works with $\phi_0 = 3\pi/4$, with as low as 100 kV/gap (lower three curves)



1076 3.1.4 Extraction

1077 From $R = p/qB$ and assuming constant field (legitimate in the presence of a very
1078 small field index), with kinetic energy $E_k = p^2/2M$ in the non-relativistic approxi-
1079 mation ($E_k \ll M$), one gets

$$\frac{dR}{R} = \frac{1}{2} \frac{dE_k}{E_k} \quad (3.28)$$

1080 Integrating the right hand side equality yields

$$R^2 = R_0^2 \frac{E_k}{E_{k,0}} \quad (3.29)$$

1081 with $R_0, E_{k,0}$ initial conditions. From Eqs. 3.28, 3.29, assuming $E_{k,0} \ll E_k$ and
1082 constant acceleration rate dE_k such that $E_k = n dE_k$ after n turns, one gets the
1083 scaling laws

$$R \propto \sqrt{n}, \quad dR \propto \frac{R}{E_k} \propto \frac{1}{R} \propto dE_k, \quad \frac{dR}{dn} = \frac{R}{2n} \quad (3.30)$$

1084 so that, in particular, the turn separation dR/dn is proportional to the average orbit
1085 radius R and to the energy gain per turn.

1086 The radial distance between successive turns decreases with energy, toward zero
1087 (Fig. 3.16), eventually resulting in insufficient spacing for insertion of an extraction
1088 septum.

1089 *Betatron modulation*

1090 Consider a particle bunch injected in the cyclotron with some (x_0, x_0') conditions, and
1091 assume very slow acceleration. While accelerated the bunch undergoes a betatron
1092 motion around the local closed orbit, following Eq. 3.15. Observed at some azimuth

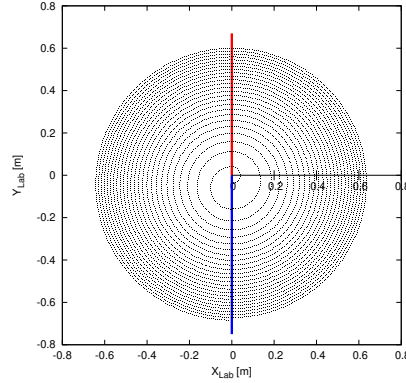


Fig. 3.16 The radial distance between successive turns decreases with energy, in inverse proportion to the orbit radius

1093 *s*, this betatron oscillation modulates the distance of the bunch to the local reference
 1094 closed orbit, moving it outward or inward depending on the turn number, which
 1095 means a modulation of the distance between the accelerated turns: an effect that
 1096 can be exploited for increasing the separation of consecutive orbits at extraction to
 1097 enhance the extraction efficiency [8].

1098 3.1.5 Spin Dance

1099 An effect of a magnetic field \mathbf{B} on a spin angular momentum \mathbf{S} , as a consequence of
 1100 the resulting torque, is the spin precession, around the precession vector (Sec. 18.6.1)

$$\omega_{\text{sp}} = \frac{q}{m} [\mathbf{B} + G(\mathbf{B}_{\parallel} + \gamma\mathbf{B}_{\perp})] \quad (3.31)$$

1101 at an angular frequency $|\omega_{\text{sp}}|$, with $\mathbf{B} = \mathbf{B}_{\parallel} + \mathbf{B}_{\perp}$, \mathbf{B}_{\parallel} and \mathbf{B}_{\perp} the magnetic field
 1102 components respectively parallel and normal to the particle velocity, and G the
 1103 anomalous gyromagnetic factor:

$$1104 \quad G=1.7928474 \text{ (proton)}, -0.178 \text{ (Li)}, -0.143 \text{ (deuteron)}, -4.184 \text{ (}^3\text{He)} \dots$$

1105 The spin precession in \mathbf{B} satisfies the Thomas-BMT differential equation

$$\frac{d\mathbf{S}}{dt} = \mathbf{S} \times \omega_{\text{sp}} \quad (3.32)$$

1106 If the particle moves in the median plane of a cyclotron then $\mathbf{B}_{\parallel} = 0$ and the
 1107 precession axis is parallel to the magnetic field vector, \mathbf{B}_y , namely $\omega_{\text{sp}} = \frac{q}{m} (1 +$
 1108 $G\gamma)\mathbf{B}_y$. The precession angle writes

$$\theta_{\text{sp, Lab}} = \frac{1}{v} \int \omega_{\text{sp}} ds = (1 + G\gamma) \frac{\int B ds}{BR} = (1 + G\gamma)\alpha \quad (3.33)$$

with α the trajectory bend angle (Fig. 3.17). The precession angle in the moving

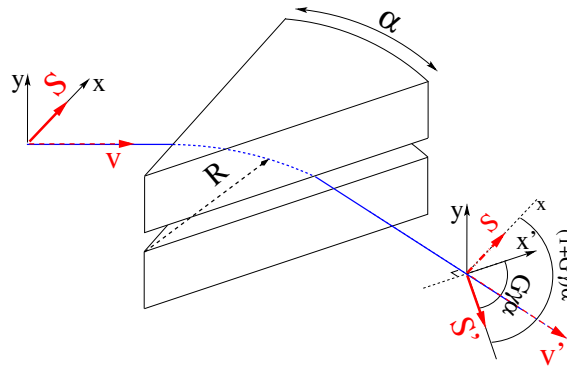


Fig. 3.17 Spin and velocity vector precession in a constant field, from \mathbf{S} to \mathbf{S}' and \mathbf{v} to \mathbf{v}' respectively. In the moving frame the spin precession along the arc $\mathcal{L} = R\alpha$ is $G\gamma\alpha$, in the laboratory frame the spin precesses by $(1 + G\gamma)\alpha$

1109

1110 frame (the latter rotates by an angle α across the magnet) is

$$\theta_{\text{sp}} = G\gamma\alpha \quad (3.34)$$

1111 from what it results that the number of precessions per turn is $G\gamma$. By analogy with
 1112 the betatron tune (the number of sinusoidal oscillations per turn around the reference
 1113 circle, Eq. 3.17) this defines the spin tune

$$\nu_{\text{sp}} = G\gamma \quad (3.35)$$

1114 3.2 Exercises

1115 Preliminaries

- 1116 • Zgoubi users' guide at hand, when setting up the input data files to work out
1117 the exercises, is a must-have. PART B of the guide in particular, details the
1118 formatting of the input data lists following keywords (a few keywords only, for
1119 instance FAISCEAU, MARKER, YMY, do not require additional data), and gives
1120 the units to be used.
- 1121 • Regarding keywords: by "keyword" it is meant, the name of the optical elements,
1122 or I/O procedures, or commands, as they appear in a simulation input data file.
1123 Keywords are most of the time referred to without any additional explanation: it
1124 is understood that the users' guide is at hand, and details regarding the use and
1125 functioning to be sought there: in PART A of the guide, as to what a particular
1126 keyword does and how it does it; in PART B as to the formatting of the data
1127 list under a particular keyword. The users' guide INDEX is a convenient tool to
1128 navigate amongst keywords. A complete list may also be found in the "Glossary
1129 of Keywords", at the beginning of both PART A and PART B of the users' guide,
1130 and an overview of what they can be used at is given in "Optical elements versus
1131 keywords".
- 1132 – The concise notation KEYWORDS[ARGUMENT1, ARGUMENT2, ...] used
1133 in the exercise: it follows the nomenclature of the Users' Guide, Part B. Con-
1134 sider a couple of examples:
 - 1135 · OBJET[KOBJ=1] stands for keyword OBJET, and the value of KOBJ=1
1136 retained here;
 - 1137 · OPTIONS[CONSTY=ON] stands for keyword OPTIONS, and the option
1138 retained here, CONSTY, switched ON.
- 1139 – The keyword INCLUDE is used in many simulation input data files. The
1140 reason is mostly to reduce the length of these files (which would otherwise
1141 be prohibitively voluminous). Just as with the Latex, or Fortran, "include"
1142 command, a segment of an optical sequence subject to an INCLUDE may
1143 always be replaced by that very sequence segment.
- 1144 • Coordinate Systems: two sets of coordinate notations are used in the exercises,
 - 1145 – on the one hand (and, in the Solutions Section mostly), zgoubi's (Y,T,Z,P,X,D)
1146 coordinates in the optical element reference frame (O;X,Y,Z), the very frame
1147 in which the optical element field $\mathbf{E}(X, Y, Z)$ and/or $\mathbf{B}(X, Y, Z)$ is defined (the
1148 origin for X depends on the optical element). Particle coordinates in this frame
1149 can be
 - 1150 · either Cartesian, in which case X, Y (angle T) and Z (angle P) denote
1151 respectively the longitudinal, transverse horizontal and vertical coordinates,
 - 1152 · or cylindrical, in which case, given m the projection of particle position M
1153 in the $Z=0$ plane, Y denotes the radius: $Y = |\mathbf{Om}|$, whereas X denotes the

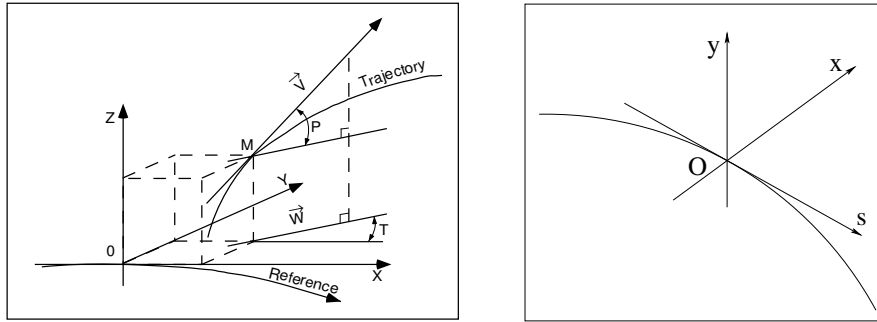


Fig. 3.18 Zgoubi Cartesian frame (O;X,Y,Z), and moving frame (O;s,x,y)

1154 **OX-Om** angle (and, yes, the nature of the variables named X and Y in the
1155 source code does change);

Note: the sixth zgoubi's coordinate above is

$$D = \frac{\text{particle rigidity}}{BORO}$$

1156 with BORO a reference rigidity, the very first numerical datum to appear in
1157 any zgoubi sequence, as part of the definition of initial particle coordinates by
1158 OBJET or MCOBJET. BORO may sometimes be denoted $B\rho_{\text{ref}}$, depending
1159 upon the context. Note that D-1 identifies with the above $\delta p/p$.

1160 – on the other hand (and, in the exercise assignments mostly), the conventional
1161 $(x,x',y,y',\delta l,\delta p/p)$ coordinates in the moving frame (O;s,x,y) or close variants.

1162 Comments are introduced wherever deemed necessary (hopefully, often enough)
1163 in an effort to lift potential ambiguities regarding coordinate notations.

1164 3.1 Modeling a Cyclotron Dipole: Field Map

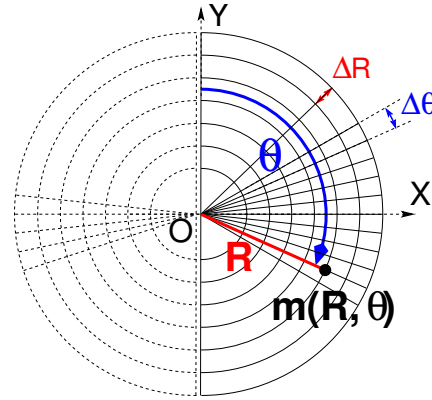
1165 In this exercise, a cyclotron dipole field is simulated using a field map. A field
1166 map is an easy way to simulate a magnet, this is a major interest of the method. It can
1167 account for fancy geometries and fields, including field index and non-linearities,
1168 field defects. Depending on field symmetries it may be 1-, 2-, or 3-dimensional. It can
1169 be generated using mathematical field models, or from magnet computation codes, or
1170 from magnetic measurements. In this exercise a model of a cyclotron field is devised
1171 using such field map method. The model is based on a calculated two-dimensional
1172 map of the mid-plane field, with 180 deg or 60 deg angular extent; TOSCA keyword
1173 is used to raytrace through these maps.

1174 The first step in this exercise consists in fabricating that field map.

1175 A 2-dimensional $m(R, \theta)$ polar meshing of the median plane is considered
1176 (Fig. 3.19). It is defined in a (O; X, Y) frame and covers a 180^0 sector (or 60 deg, in
1177 some of the exercises). The median plane field map provides the values of the field
1178 components $B_Z(R, \theta)$ normal to the $Z = 0$ plane, at the nodes of the mesh. Note

1179 that a single 360° field map could be used instead, however implementing two 180°
 1180 sectors will allow further insertion of an accelerating gap, between the two 180°
 1181 sectors. Computation of the field along (R, θ) particle trajectories in the $(O; X, Y, Z)$
 1182 frame is performed from the field map data, using interpolation techniques [13].

Fig. 3.19 Principle of a field map in a polar coordinate system, covering a 180° sector (over the right hand side dee). The mesh nodes $m(R, \theta)$ are distant ΔR radially, $\Delta\theta$ azimuthally. The map is used twice, so covering the 360° cyclotron dipole as sketched here, while allowing further insertion of an accelerating gap between the two dees



1183 (a) Construct a 180° two-dimensional map of a median plane field $B_Z(R, \theta)$,
 1184 proper to simulate the field in a cyclotron as sketched in Fig. 3.1. Use a uniform
 1185 mesh in a polar coordinate system (R, θ) as sketched in Fig. 3.19, covering from $R=1$
 1186 to 76 cm. Take a radial increment of the mesh $\Delta R = 0.5$ cm, azimuthal increment
 1187 $\Delta\theta = 0.5$ cm/RM, RM some arbitrary reference radius (say, 50 cm, here), and
 1188 constant axial field $B_Z = 0.5$ T. The appropriate 6-column formatting of the field
 1189 map data for TOSCA to read them is the following:

$$R \cos \theta, Z, R \sin \theta, B_Y, B_Z, B_X$$

1191 with θ varying first, R varying second in that list. Z is the vertical direction (normal
 1192 to the map mesh), $Z \equiv 0$.

1193 Produce a graph of $B_Z(R, \theta)$.

1194 (b) Raytrace a few concentric circular mid-plane trajectories centered on the
 1195 center of the dipole, ranging in $10 \leq R \leq 80$ cm. Produce a graph of these concentric
 1196 trajectories in the $(O; X, Y)$ laboratory frame. Initial coordinates can be defined using
 1197 OBJET, particle coordinates along trajectories during the stepwise raytracing can be
 1198 logged in zgoubi.plt by setting IL=2 under TOSCA.

1199 Explain why it is possible to push the raytracing beyond the 76 cm radius field
 1200 map extent, without loss of accuracy.

1201 (c) Compute the orbit radius R and the revolution period T_{rev} as a function of
 1202 kinetic energy E_k , or rigidity BR . Produce a graph, including for comparison the
 1203 theoretical dependence of T_{rev} . Explain what causes the slow increase of revolution
 1204 period with energy.

1205 (d) Check the effect of the density of the mesh (the choice of ΔR and $\Delta\theta$ values,
 1206 *i.e.*, the number of nodes $N_\theta \times N_R = (1 + \frac{180^\circ}{\Delta\theta}) \times (1 + \frac{80 \text{ cm}}{\Delta R})$), on the accuracy of the
 1207 trajectory and time-of-flight computation.

1208 (e) Consider a mesh with such ΔR , $\Delta\theta$ density as to ensure reasonably good
 1209 convergence of the numerical resolution of the differential equation of motion [13,
 1210 Eq. 1.2.4].

1211 Check the effect of the integration step size on the accuracy of the trajectory
 1212 and time-of-flight computation, by considering a small $\Delta s = 1$ cm and a large
 1213 $\Delta s = 20$ cm, at 200 keV and 5 MeV (assume proton).

1214 (f) Consider a periodic orbit, thus its radius R should remain unchanged after
 1215 stepwise integration of the motion over a turn. However, the size Δs of the numerical
 1216 integration step has an effect on the final value of the radius:

1217 for two different cases, 200 keV (a small orbit) and 5 MeV (a larger one), provide
 1218 the dependence of the relative error $\delta R/R$ after one turn, on the integration step size
 1219 Δs (consider a series of Δs values in a range $\Delta s : 0.1$ mm \rightarrow 20 cm). Plot the two
 1220 $\frac{\delta R}{R}(\Delta s)$ curves (200 keV and 5 MeV), explain their upward concavity.

1221 3.2 Modeling a Cyclotron Dipole: Analytical

1222 This exercise is similar to exercise 3.1, the difference is that an analytical modeling
 1223 of the field is used here, rather than a field map. The same polar coordinate system
 1224 (R, θ, Z) is considered, with vertical axis Z normal to the (R, θ) plane (Fig. 3.20).

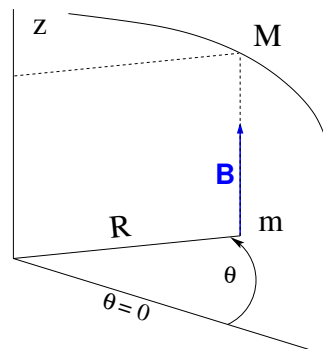


Fig. 3.20 Polar frame.
 DIPOLE provides the value $B_z(m)$ of the median plane field at m , projection of particle position $M(R, \theta, Z)$ in the median plane (R, θ)

1225 The vector field $\mathbf{B}(R, \theta, Z)$ at any location $M(R, \theta, Z)$ of a particle along its
 1226 trajectory is modeled using DIPOLE (a convenient choice among other possibilities
 1227 found in zgoubi optical element library). DIPOLE provides the Z -parallel median
 1228 plane field $\mathbf{B}(R, \theta, Z = 0) \equiv \mathbf{B}_z(R, \theta, Z = 0)$, and $\mathbf{B}(R, \theta, Z)$ off the median plane is
 1229 obtained by Taylor expansion (accounting for Maxwell's equations).

1230 (a) Simulate a 180° sector dipole; DIPOLE requires a reference radius, R_M , for
 1231 the sake of consistency with other exercises, it is suggested to take $R_M=50$ cm. Take
 1232 a constant axial field $B_z = 0.5$ T.

1233 Explain the various data (geometry, role of R_M , field and field indices, fringe
 1234 fields, integration step size, etc.) that define the field simulation in DIPOLE - refer
 1235 to the Users' Guide [13].

1236 Produce a graph of $B_z(R, \theta)$.

1237 (b) Repeat question (b) of exercise 3.1.

1238 (c) Repeat question (c) of exercise 3.1.

1239 (d) As in question (e) of exercise 3.1, check the effect of the integration step size
1240 on the accuracy of the trajectory and time-of-flight computation.

1241 Repeat question (f) of exercise 3.1.

1242 (e) From the two series of results (exercise 3.1 and the present one), comment on
1243 various pros and cons of the two methods, field map versus analytical field model.

1244 3.3 Geometrical Focusing

1245 Because the field is constant over the all space ($\mathbf{B} \equiv \mathbf{B}_Z$ and $|\mathbf{B}_Z| = \text{constant}$, \forall
1246 X, Y, Z), there is no vertical focusing: any trajectory with a non-zero vertical angle
1247 would spiral away, vertically, with constant pitch angle.

1248 (a) Using the foregoing field model, verify that this is what the numerical inte-
1249 gration yields.

1250 Produce a 3-D graph of the trajectory, superpose theory (use the parametric
1251 equations of motion) and numerical integration.

1252 (b) Instead, horizontal motion features geometrical focusing, this is due to the
1253 trajectory curvature. Show the geometrical focusing graphically.

1254 3.4 Relativistic Kinematic Relationships

1255 In the subsequent exercises, relativistic kinematic quantities will be used, this
1256 exercises introduces some differential relations between them which will also be
1257 resorted to.

1258 (a) Demonstrate the following relativistic relations (M =rest mass, E_k =kinetic
1259 energy, $E = E_k + M$, $c=1$; γ may vary in electrostatic elements or in the RF cavities
1260 of an accelerator):

$$1261 \frac{dp}{p} = \frac{1}{\beta^2} \frac{dE}{E}, \quad dp = \frac{dE}{\beta}$$

$$1262 \frac{dv}{v} = \frac{d\beta}{\beta} = \frac{1}{\gamma^2} \frac{dp}{p} = \frac{1}{\beta^2 \gamma^2} \frac{dE}{E} = \frac{1}{\beta^2 \gamma^2} \frac{d\gamma}{\gamma}$$

$$1263 \frac{d\gamma}{\gamma} = \frac{dE}{E} = \frac{dM\gamma}{M\gamma} = \frac{dE_k}{E_k + M}$$

$$1264 \frac{dE}{E - M} = \frac{dE_k}{E_k} = \frac{\gamma + 1}{\gamma} \frac{dp}{p}$$

1265 (b) Produce the evolution of these quantities numerically, compare these numeri-
1266 cal results with theoretical expectations from (a).

1267 (c) Using the random particle generator MCOBJET, produce a 2×10^4 bunch
1268 of protons with Gaussian dp/p , $\sigma_{dp/p} = 10^{-3}$. Plot some of the densities above and
1269 check the equalities in (a).

1270 3.5 Resonant Acceleration

1271 Based on the earlier dipole sector, using indifferently a field map or an analytical
1272 model of the field, introduce an accelerating gap between the two dees with peak
1273 voltage 100 kV. Assume that particle motion does not depend on RF phase: the boost
1274 through the gap is the same at all passes, CAVITE[IOPT=3] can be used for that.

1275 (a) Accelerate a proton with initial kinetic energy 20 keV, up to 5 MeV, take
 1276 harmonic $h=1$. Produce a graph of the accelerated trajectory in a (O; X, Y) frame
 1277 similar to that in Fig. 3.19.

1278 (b) Plot the proton momentum p and total energy E as a function of its kinetic
 1279 energy, both from this numerical experiment (raytracing data can be stored using
 1280 FAISTORE) and from theory, everything on the same graph.

1281 (c) Plot the normalized velocity $\beta = v/c$ as a function of kinetic energy, both
 1282 numerical and theoretical, and in the latter case both classical and relativistic.

1283 (d) Plot the relative change in velocity $\Delta\beta/\beta$ and the relative change in circum-
 1284 ference $\Delta C/C$, as a function of kinetic energy. both numerical and theoretical. From
 1285 their evolution, conclude that the time of flight increases with energy.

1286 3.6 Resonant Acceleration (2)

1287 Re-do the previous exercise, assuming a harmonic $h=3$ RF frequency.

1288 3.7 Visit High Energies

1289 Forget the fact that this not possible in a classical cyclotron (use CAVITE[IOPT=3]),
 1290 and push proton energy to 3 GeV kinetic, re-do questions (a) to (d) of Ex. 3.5.

1291 Note:

1292 - pushing the energy in this manner is only possible if acceleration at the gap is
 1293 independent of particle phase, hence the necessary choice of CAVITE[IOPT=3],

1294 - if a field map model is used, it is perhaps, or perhaps not, necessary to extend the
 1295 radial extent of the mesh to encompass the spiraling trajectory up to 3 GeV - please
 1296 clarify that point,

1297 - in the case the analytical model DIPOLE is used instead, surely no modification
 1298 is needed, its data remain unchanged, figure that out.

1299 3.8 Spin Dance

1300 (a) From the analogy between the vector precession equations,

$$1301 \quad \dot{\mathbf{v}} = \frac{q}{m} \mathbf{v} \times \mathbf{B}, \quad \text{particle velocity vector, on the one hand}$$

$$1302 \quad \dot{\mathbf{S}} = \mathbf{S} \times \boldsymbol{\omega}_{\text{sp}}, \quad \text{particle spin vector, on the other hand (Eq. 18.28),}$$

1303 and from the expression for the particle trajectory rotation angle $\alpha = \int B ds / BR$ as
 1304 stems from the former, deduce the expression for the spin rotation angle in constant
 1305 vertical B field - no calculations needed.

1306 In the following the cyclotron model of exercise 3.1 or 3.2 indifferently can be
 1307 used.

1308 (b) Add spin transport, using SPNTRK. Produce a listing (zgoubi.res) of a simu-
 1309 lation, including spin outcomes.

1310 Note: PARTICUL is necessary here, in order for the equation of motion to be
 1311 solved [13, Sec. 2]. SPNPRT can be used to have local spin coordinates listed in
 1312 zgoubi.res (at the manner FAISCEAU lists particle coordinates).

1313 (c) Consider proton case, initial spin longitudinal, compute the spin precession
 1314 over one revolution, as a function of energy over a range 12 keV \rightarrow 5 MeV. Give a
 1315 graphical comparison with theory.

1316 FAISTORE can be used to store local particle data, which include spin coordi-
 1317 nates, in a zgoubi.fai style output file. IL=2 can be used to obtain a print out of
 1318 particle motion data to zgoubi.plt during stepwise integration.

1319 (d) Inject a proton with longitudinal initial spin S_z . Give a graphic of the longi-
 1320 tudinal spin component motion as a function of azimuthal angle, over a few turns
 1321 around the ring. Deduce the spin tune from this computation. Repeat for a couple of
 1322 different energies.

1323 Place both FAISCEAU and SPNPRT commands right after the first dipole sector,
 1324 and use them to check the spin rotation and its relationship to particle rotation, right
 1325 after the first passage through that first sector.

1326 (e) Spin dance: the optical sequence here is assumed to be a complete turn (*i.e.*,
 1327 six DIPOLES if a 60 deg DIPOLE model is used). Inject an initial spin at an angle
 1328 from the horizontal plane (this is in order to have a non-zero vertical component),
 1329 produce a 3-D animation of the spin dance around the ring, over a few turns.

1330 (f) Repeat questions (b-e) for two additional particles: deuteron (much slower
 1331 spin precession), ${}^3\text{He}^{2+}$ (much faster spin precession).

1332 3.9 Synchronized Spin Torque

1333 A synchronized spin kick is superimposed on orbital motion. A input data file
 1334 accounting the simulation of a complete cyclotron is considered as in (e), for
 1335 instance six 60 degree DIPOLES, or two 180 degree DIPOLES, etc.

1336 Insert a spin rotation of a few degrees around the longitudinal axis, at the end
 1337 of the optical sequence (*i.e.*, after one orbit around the cyclotron). SPINR can be
 1338 used for that, to avoid any orbital effect. Track 4 particles on their closed orbit, with
 1339 respective energies 0.2, 108.412, 118.878 and 160.746 MeV.

1340 Produce a graph of the motion of the vertical spin component S_y along the circular
 1341 orbit.

1342 Produce a graph of the spin vector motion on a sphere.

1343 Explain the results.

1344 3.10 Introducing a Radial Field Index

1345 (a) Reproduce Fig. 3.11.

1346 (b) Ray trace over a few turns with some $-1 < k < 0$ value, to show the sinusoidal
 1347 horizontal motion. Show the horizontal motion instability when $k < -1$.

1348 (c) Add vertical motion and show the vertical sinusoidal oscillation with $k < 0$,
 1349 show the vertical instability if $k > 0$.

1350 3.11 Weak Focusing

1351 (a) Consider a 60° sector as in earlier exercises (building a field map as in
 1352 exercise 3.1, or using DIPOLE as in exercise 3.2), construct the sector accounting
 1353 for a non-zero radial index k in order to introduce vertical focusing, say $k = -0.03$,
 1354 assume a reference radius R_0 for a reference energy of 200 keV (R_0 and B_0 are
 1355 required in order to define the index k , Eq. 3.12). Raytrace that 200 keV reference
 1356 orbit, plot it in the lab frame: make sure it comes out as expected, namely, constant
 1357 radius, final and initial angles equal (normally null given the working hypotheses, as
 1358 established in previous exercises).

1359 (b) Find and plot the radius dependence of orbit rigidity, $BR(R)$, from raytracing
1360 over a BR range covering 20 keV to 5 MeV.

1361 (c) Produce a graph of the paraxial axial motion of a 1 MeV proton, over a
1362 few turns (use $IL=2$ under TOSCA to have stepwise integration data logged in
1363 `zgoubi.plt`). Check the effect of the focusing strength by comparing the trajectories
1364 for a few different index values, including close to -1 and close to 0.

1365 (d) Produce a graph of the magnetic field experienced by the particle along these
1366 trajectories.

1367 3.12 Loss of Isochronism

1368 Compare on a common graphic the revolution period $T_{rev}(R)$ for a field index
1369 value $k \approx -0.95, -0.5, -0.03, 0^-$. The scan method of exercise 3.11, based on
1370 REBELOTE, can be referred to.

1371 3.13 Particle Trajectories

1372 In this exercise individual particle trajectories are computed. DIPOLE or TOSCA
1373 can be used, indifferently. No acceleration in this exercise, particles cycle around the
1374 cyclotron at constant energy.

1375 (a) Produce a graph of the horizontal and vertical trajectory components $x(s)$ and
1376 $y(s)$ of a particle with rigidity close to $BR(R_0)$ (R_0 is the reference radius in the
1377 definition of the index k), over a few turns around the cyclotron. From the number of
1378 turns, give an estimate of the wave numbers. Check the agreement with the expected
1379 $\nu_R(k), \nu_y(k)$ values from Eq. 3.17.

1380 Consider particle energies of 1 MeV and 5 MeV, far from the reference kinetic
1381 energy $E(R_0)$; the wave numbers change with energy: could that be expected? Find
1382 their theoretical values, compare with numerical outcomes.

1383 (b) In the former case, 200 keV energy, plot as a function of s the difference
1384 between $x(s)$ from raytracing and its values from Eq. 3.15. Same for $y(s)$ compared
1385 to Eq. 3.16. Is there agreement? (use the option $IL=2$ to store particle coordinates in
1386 `zgoubi.plt`, step-by-step).

1387 3.14 Energy Dependence of Wave Numbers

1388 Perform a scan of the wave numbers over 200 keV–5 MeV energy interval, com-
1389 puted using MATRIX, and using REBELOTE to repeat MATRIX computation for
1390 a series of energy values.

1391 3.15 Phase Space Motion, Fourier Analysis

1392 This exercise introduces to phase space and phase space motion, and to spectral
1393 analysis of particle motion.

1394 Raytrace a particle with small amplitude radial and axial oscillations with respect
1395 to the reference circular closed orbit (paraxial motion), at constant energy.

1396 (a) At some fixed azimuth s around the cyclotron, observe the radial excursion
1397 $(x(n), x'(n))$ of the particle as it cycles around for many turns (n is the turn number)
1398 (use FAISTORE to store particle coordinates in `zgoubi.fai`, turn by turn). Produce a
1399 graph of $(x(n), x'(n))$ in the transverse phase-space (x, x') .

1400 Repeat for (y, y') .

1401 (b) From the trajectory equation (Eq. 3.15, radial motion, or Eq. 3.16, axial
 1402 motion), show that particle motion in phase space is on an ellipse. Calculate the
 1403 ellipse parameters. Verify graphically that it superposes on the particle motion from
 1404 multiturn raytracing.

1405 (c) Compute the radial and axial wave numbers by Fourier analysis of respectively
 1406 the $x(n)$ and the $y(n)$ motion. Check the agreement with the expected $\nu_R(k)$, $\nu_y(k)$
 1407 values from theory.

1408 (d) Constant energy motion spectrum:

1409 (i) there is an indetermination on the value of the wave number, from the Fourier
 1410 analysis, explain

1411 (ii) give a theoretical calculation of the accuracy on the position of the peak from
 1412 the DFT technique. Check this against the numerical computation by varying the
 1413 spectrum sampling in the DFT series

1414 (iii) explain the origin of the $\sin u/u$ shape of the spectrum. Calculate the spacing
 1415 between the zeroes, from theory, compare with the zeroes of the numerical DFT.

1416 3.16 RF Phase at the Accelerating Gap

1417 (a) Consider the cyclotron model of exercise 3.11: two dees, double accelerating
 1418 gap, field index $k = -0.03$ defined at $R_0 = 50$ cm, field $B_0 = 5$ kG on that radius.

Raytrace a proton trajectory from 1 to 5 MeV: get the turn-by-turn phase-shift at
 the gaps, compare with (Eq. 3.26)

$$\text{half-turn } \Delta\phi = \pi \left(\frac{\omega_{rf}}{\omega_{rev}(R)} - 1 \right) = \pi \left(\frac{m\omega_{rf}}{qB(R)} - 1 \right)$$

1419 Produce a similar diagram $\Delta W(\phi)$ to Fig. 3.14-right.

1420 Accelerate over more turns, observe the particle decelerate.

1421 (b) Repeat (a) for the index definition of exercise 3.11: $k=-0.03$, defined on the
 1422 200 keV injection radius $R_0 = 12.924888$ cm, with $B_0 = 5$ kG.

1423 3.17 The Cyclotron Equation

1424 Cyclotron model settings of exercise 3.5 are first considered in questions (a) to (c):
 1425 two dees, double accelerating gap, uniform field $B = 0.5$ T (a field map or analytical
 1426 field modeling can be used, indifferently). In question (d) a field index is introduced.

1427 (a) Set up an input data file for the simulation of a proton acceleration from
 1428 0.2 to 20 MeV. In particular, assume that $\cos(\phi)$ reaches its maximum value at
 1429 $W_m = 10$ MeV; find the RF voltage frequency from $d(\cos \phi)/dW = 0$ at W_m .

(b) Give a graph of the energy-phase relationship (Eq. 3.27)

$$\cos \phi = \cos \phi_0 + \pi \left[1 - \frac{\omega_{rf}}{\omega_{rev}} \frac{E + E_0}{2M} \right] \frac{E - E_0}{q\hat{V}}$$

1430 for $\phi_0 = \frac{3\pi}{4}, \frac{\pi}{2}, \frac{\pi}{4}$, from both simulation and theory.

1431 (c) Re-do the exercise using an RF frequency third harmonic of the revolution
 1432 frequency, in the same double-dee configuration.

1433 (d) Repeat (a) and (b) for the index definition of exercise 3.11: $k=-0.03$, defined
 1434 on the 200 keV injection radius $R_0 = 12.924888$ cm, with $B_0 = 5$ kG.

1435 **3.18 Cyclotron Extraction**

1436 (a) Acceleration of a proton in a uniform field $B=0.5$ T is first considered, this is
1437 the case of exercise 3.5.

1438 Compute the distance ΔR between turns, as a function of turn number and of
1439 energy, over the range $E : 0.02 \rightarrow 5$ MeV. Compare graphically with theoretical
1440 expectation.

1441 (b) Assume a beam with Gaussian momentum distribution and *rms* momentum
1442 spread $\delta p/p = 10^{-3}$. An extraction septum is placed half-way between two successive
1443 turns, plot the percentage of beam loss at extraction, as a function of extraction turn
1444 number - COLLIMA can be used for that simulation and for particle counts, it also
1445 allows for possible septum thickness.

1446 (c) Repeat (a) and (b) considering a field with index - conditions of exercise 3.10
1447 for instance, $B_0 = 0.5$ T and $k = -0.03$ at $R_0 = R(0.2 \text{ MeV}) = 12.924888$ cm.

1448 (d) Investigate the effect of injection conditions (x_0, x'_0) on the modulation of the
1449 distance between turns.

1450 Show that, with slow acceleration, the oscillation is minimized for an initial
1451 $|x'_0| = \left| \frac{x_0 v R}{R} \right|$ [8, p. 133].

1452 **3.19 Acceleration and Extraction of a 6-D Polarized Bunch**

1453 The cyclotron simulation hypotheses of exercise 3.17-a are considered.

1454 Add a short “high energy” line, say 1 meter, for beam extraction downstream of
1455 the cyclotron (which means following REBELOTE in the optical sequence), ending
1456 up with a “Beam_Dump” MARKER.

1457 (a) Create a 1,000 particle bunch with the following initial parameters:

1458 - random Gaussian transverse phase space densities, centered on the closed orbit,
1459 truncated at 3 sigma, normalized *rms* emittances $\epsilon_Y = \epsilon_Z = 1 \pi \mu\text{m}$, both emittances
1460 matched to the 0.2 MeV orbit optics,

1461 - uniform bunch momentum density $0.2 \times (1 - 10^{-3}) \leq p \leq 0.2 \times (1 + 10^{-3})$ MeV,
1462 matched to the dispersion, namely (Eq. 3.21), $\Delta x = D \frac{\Delta p}{p}$,

1463 - random uniform longitudinal distribution $-0.5 \leq s \leq 0.5$ mm,

1464 Note: there is two possibilities to create this object, namely, using either
1465 (i) MCOBJET, or (ii) OBJET[KOBJ=3] which reads an external file containing
1466 particle coordinates.

1467 Add spin tracking request (SPNTRK), all initial spins normal to the bend plane.

1468 Produce a graph of the three initial 2-D phase spaces: (Y,T), (Z,P), $(\delta l, \delta p/p)$,
1469 check the matching to the 200 keV optics.

1470 Plot the Y, Z, dp/p , δl and S_Z histograms. Check the distribution parameters.

1471 (b) Accelerate this polarized bunch to 20 MeV, using the following RF conditions:

1472 - 200 kV peak voltage,

1473 - RF harmonic 1,

1474 - initial RF phase $\phi_0 = \pi/4$.

1475 Produce a graph of the three phase spaces as observed downstream of the ex-
1476 traction line. Plot the Y, Z, dp/p , δl and S_Z histograms. Compare the distribution
1477 parameters with the initial values.

1478 What causes the spins to spread away from vertical?

References

- 1480 1. Jones, L., Mills, F., Sessler, A., et al.: Innovation Was Not Enough. World Scientific (2010)
- 1481 2. Lawrence, E.O., Livingston, M.S., Phys. Rev. 37, 1707 (1931), 1707; Phys. Rev. 38, 136,
- 1482 (1931); Phys. Rev. 40, 19 (1932)
- 1483 3. Ernest O. Lawrence and M. Stanley Livingston, The Production of High Speed Light Ions
- 1484 Without the Use of High Voltages, Phys. Rev. 40, 19-35 (1932)
- 1485 4. Livingston, M.S., McMillan, Edwin M.: History of the cyclotron. Physics Today, 12(10)
- 1486 (1959).
- 1487 <https://escholarship.org/uc/item/29c6p35w>
- 1488 5. Bethe, H. E., Rose, M. E.: Maximum energy obtainable from cyclotron. Phys. Rev. 52 (1937)
- 1489 1254
- 1490 6. Cole, F.T.: O Camelot ! A memoir of the MURA years (April 1, 1994).
- 1491 <https://accelconf.web.cern.ch/c01/cyc2001/extra/Cole.pdf>
- 1492 7. 4.a L.H.Thomas, *The Paths of Ions in the Cyclotron*, Phys. Rev. 54, 580, (1938)
- 1493 4.b M.K. Craddock, *AG focusing in the Thomas cyclotron of 1938* , Proceedings of PAC09,
- 1494 Vancouver, BC, Canada, FR5REP1
- 1495 8. Stambach, T.: Introduction to Cyclotrons. CERN accelerator school, cyclotrons, linacs and
- 1496 their applications. IBM International Education Centre, La Hulpe, Belgium, 28 April-5 May
- 1497 1994.
- 1498 9. Baron, E., et al.: The GANIL Injector. Proceedings of the 7th International Conference on
- 1499 Cyclotrons and their Applications, ZÄijrich, Switzerland (1975).
- 1500 <http://accelconf.web.cern.ch/c75/papers/b-05.pdf>
- 1501 10. Li, C.Y., et al.: A Permanent Magnet System for a Cyclotron used as a mass spectrometer.
- 1502 11. Lawrence, E.O., Edlefsen, N.E.: On the production of high speed protons. Science, 72, 376-377
- 1503 (1930)
- 1504 12. Le Duff, J.: Longitudinal beam dynamics in circular accelerators. CERN Accelerator School,
- 1505 Jyvaskyla, Finland, 7-18 September 1992
- 1506 13. Méot, F.: Zgoubi Users' Guide.
- 1507 <https://www.osti.gov/biblio/1062013-zgoubi-users-guide> Sourceforge latest version:
- 1508 <https://sourceforge.net/p/zgoubi/code/HEAD/tree/trunk/guide/Zgoubi.pdf>